

**2001-GT-0265**

## NUMERICAL INVESTIGATION OF BLADE FLUTTER AT OR NEAR STALL IN AXIAL FLOW TURBOMACHINES

**Wolfgang Höhn**

MTU Aero Engines

Department of Aeroelasticity and Acoustics

Dachauer Straße 665, D-80995 München

Germany

Email: wolfgang.hoehn@muc.mtu.de

### ABSTRACT

During the design of the compressor and turbine stages of today's aeroengines, aerodynamically induced vibrations become increasingly important since higher blade load and better efficiency are desired. In this paper the development of a method based on the unsteady, compressible Navier-Stokes equations in two dimensions is described in order to study the physics of flutter for unsteady viscous flow around cascaded vibrating blades at stall.

The governing equations are solved by a finite difference technique in boundary fitted coordinates. The numerical scheme uses the Advection Upstream Splitting Method to discretize the convective terms and central differences discretizing the viscous terms of the fully non-linear Navier-Stokes equations on a moving H-type mesh. The unsteady governing equations are explicitly and implicitly marched in time in a time-accurate way using a four stage Runge-Kutta scheme on a parallel computer or an implicit scheme of the Beam-Warming type on a single processor. Turbulence is modelled using the Baldwin-Lomax turbulence model. The blade flutter phenomenon is simulated by imposing a harmonic motion on the blade, which consists of harmonic body translation in two directions and a rotation, allowing an interblade phase angle between neighboring blades. Non-reflecting boundary conditions are used for the unsteady analysis at inlet and outlet of the computational domain. The computations are performed on multiple blade passages in order to account for nonlinear effects. A subsonic massively stalled unsteady flow case in a compressor cascade is studied. The re-

sults, compared with experiments and the predictions of other researchers, show reasonable agreement for inviscid and viscous flow cases for the investigated flow situations with respect to the steady and unsteady pressure distribution on the blade in separated flow areas as well as the aeroelastic damping.

The results show the applicability of the scheme for stalled flow around cascaded blades. As expected the viscous and inviscid computations show different results in regions where viscous effects are important, i.e. in separated flow areas. In particular, different predictions for inviscid and viscous flow for the aerodynamic damping for the investigated flow cases are found.

### NOMENCLATURE

a	speed of sound
c	chord length
C <sub>p</sub>	pressure coefficient
f	frequency
h	bending- or torsion-amplitude
i	angle of incidence
k	reduced frequency
p	static pressure
q	velocity
t	time
u, v	fluid velocity components in the x,y direction
u <sub>τ</sub>	friction velocity
x	coordinate in axial direction
y	coordinate in circumferential direction

D diameter  
 H total enthalpy  
 J Jacobi determinant  
 L characteristic length scale  
 M Mach number  
 P pitch  
 Pr Prandtl number  
 Re Reynolds number  
 T blade passing period, temperature  
 $\alpha$  incidence angle  
 $\beta$  flow angle in moving coordinate system  
 $\delta$  partial derivative  
 $\gamma$  stagger angle, ratio of specific heats  
 $\mu$  dynamic viscosity  
 $\rho$  density  
 $\tau$  shear stress (tensor), time in computational space  
 $\alpha$  circumferential coordinate in the computational space  
 $\xi$  axial coordinate in the computational space  
 $\Phi$  flux limiter

#### Superscripts

- mean value  
 ', \* dimensionless value  
 + dimensionless turbulent value  
 $\rightarrow, -$  vector notation

#### Subscripts

t turbulent value, stagnation flow quantity  
 w value at the wall  
 L left  
 R right  
 T total value  
 $-\infty$  reference value at inlet  
 t, x, y,  $\eta$ ,  $\tau$ ,  $\xi$  partial derivative with respect to t, x, y,  $\eta$ ,  $\tau$ ,  $\xi$

## INTRODUCTION

Due to the compact design of turbomachines with higher loaded blades and increased flow temperatures and velocities, as well as improved lighter blade materials, the understanding of unsteady flow phenomena is an issue of increasing importance during the development of new gasturbines. The most important unsteady effects occurring in turbomachines are forced response and flutter. The latter denotes self-excited vibrations, which are of serious concern, because once started they can lead to the break of a blade due to high cycle fatigue causing a major damage to the whole machine. In order to understand and avoid flutter occurring in turbomachines, it is useful to have powerful prediction models to calculate the unsteady flow through cascaded blades. Then, some of the costly and time consuming experiments can be avoided and the different parameters which influence the flutter phenomena can be studied.

So far a number of methods using time-linearized models, for instance Whitehead [1990], have been developed to study

the classical blade flutter. Within such approaches the unsteady equations of motion are linearized with respect to small harmonic perturbations in time. Consequently, the unsteady surface-pressure distribution is independent of the magnitude of the small harmonic motion, i.e. in the linear range. In order to investigate realistic modern flow configurations, non-linear and viscous effects are far from negligible, especially in the vicinity of shocks as well as for shock boundary-layer interaction. Due to this circumstance the aerodynamic work of the fluid on the structure can be strongly influenced by separated flow situations in compressors and by shocks occurring in turbine cascades. Several Euler [Fransson and Pandolfi, 1986; Huff et al., 1991] and Navier-Stokes procedures [Siden, 1991] have been developed to study these flow regimes. Recent investigations using Navier-Stokes solvers [Weber et al., 1997; Ayer and Verdon, 1996] show that viscous effects cannot be neglected in particular in transonic flows regimes.

The numerical method presented here accounts for unsteady, viscous, fully turbulent flow around cascaded blades towards a better understanding of the above mentioned flow situations. It uses the "Advection Upstream Splitting Method" (AUSM) [Wada and Liou, 1994] for the discretization of the convective terms and central differences for the viscous terms of the Navier-Stokes equations. The blade flutter phenomenon is simulated by imposing a motion on the blade, which consists of harmonic body translation in two directions and rotation, allowing an interblade phase angle between two neighboring blades.

First the results for basic flow cases are shown in order to demonstrate that the developed method can resolve typical viscous flow phenomena, i.e. the viscous boundary layer and separation.

Thereafter, a compressor test case, where unsteady viscous effects occur, is investigated. The 2nd test case is a compressor cascade near stall conditions. This case serve as test in order to study the viscous effects on the unsteady pressure distribution on the blade.

The test case has not previously been investigated numerically for such high incidence angles.

## GOVERNING EQUATIONS

The presented method applies the non-dimensionalized Reynolds-averaged Navier-Stokes equations for the conservation of mass, momentum and energy and read in a boundary-fitted moving co-ordinate system [Höhn, 2000], applying a general transformation  $\xi = \xi(x, y, t)$ ,  $\eta = \eta(x, y, t)$ ,  $\tau = t$ :

$$\begin{aligned}
 & \partial_{\tau} \bar{U} + \partial_{\xi} \bar{F} + \partial_{\eta} \bar{G} \\
 & = \frac{\rho_{-\infty}^* q_{-\infty}^*}{Re_{-\infty}} (\partial_{\xi} (y_{\eta} R - x_{\eta} S)) + (\partial_{\eta} (-y_{\xi} R + x_{\xi} S))
 \end{aligned} \tag{1}$$

with

$$\begin{aligned}
\bar{U} &= \frac{U}{J}, \bar{F} = ((-x_\tau y_\eta + y_\tau x_\eta)U + y_\eta F - x_\eta G), \\
\bar{G} &= ((-x_\tau y_\xi - y_\tau x_\xi)U - y_\xi F - x_\xi G), \\
U &= \begin{pmatrix} \rho \\ \rho u \\ \rho v \\ \rho e \end{pmatrix}, F = \begin{pmatrix} \rho u \\ \rho u^2 + p \\ \rho uv \\ \rho uH \end{pmatrix}, G = \begin{pmatrix} \rho v \\ \rho uv \\ \rho v^2 + p \\ \rho vH \end{pmatrix}, \\
R &= \begin{pmatrix} 0 \\ \tau_{xx} \\ \tau_{xy} \\ u\tau_{xx} + v\tau_{xy} + \frac{\mu'}{Pr}\frac{\partial h}{\partial x} \end{pmatrix}, \\
S &= \begin{pmatrix} 0 \\ \tau_{xy} \\ \tau_{yy} \\ u\tau_{xy} + v\tau_{yy} + \frac{\mu'}{Pr}\frac{\partial h}{\partial y} \end{pmatrix}. \tag{2}
\end{aligned}$$

### Algebraic Turbulence Model

Turbulence is modelled by the algebraic turbulence model of Baldwin and Lomax [1978] after the Reynolds stresses in the Reynolds averaged Navier-Stokes equations are modelled via the Boussinesq approximation [Boussinesq, 1877; Wilcox, 1993]. In the stress terms of the laminar Navier-Stokes equations, the molecular coefficient of viscosity  $\mu$  is replaced by  $\mu + \mu_t$ . In the heat flux the term  $k/c_p = \mu/Pr$  is changed to  $\mu/Pr + \mu_t/Pr_t$ .

### Boundary Conditions

The boundary condition for the calculations is no slip at the adiabatic blade walls.

Along the inlet and outlet of the computational domain for steady state flow conditions, boundary conditions based on the theory of characteristics for the locally one-dimensional problem are used [Ott, 1991]. The unsteady computations are performed using locally non-reflecting boundary conditions [Chakravarthy, 1983]. No investigations have been made, if these boundary conditions allow small reflections or are really highly non-reflecting.

The computations are performed on multiple blade passages allowing an interblade phase angle between adjacent blades.

Details about the boundary conditions can be found in Höhn [2000].

## NUMERICAL METHOD

### Discretization of the Inviscid Terms

For the convective terms of the Reynolds-averaged Navier-Stokes equations the Advection Upstream Splitting Method (AUSM) is used. The AUSM scheme is applied on a quasi one-dimensional formulation in generalized coordinates for a moving grid. The convective flux, for example F, is splitted at the cell

face (1/2) of the computational grid according to the direction of propagation into

$$\begin{aligned}
F^{1/2} &= \frac{1}{2} \left( (\rho \bar{u}^\xi)_{1/2} (\Psi_L + \Psi_R)_{1/2} + \right. \\
&\quad \left. |(\rho \bar{u}^\xi)_{1/2}| (\Psi_L - \Psi_R)_{1/2} \right) + p_{1/2} \tag{3}
\end{aligned}$$

with  $\Psi^T = (1, u, v, H)$ .  $\Psi_{L/R}$  denote the upwind extrapolated variables, where the state vector at the cell face is obtained by upwind extrapolation, i.e. the MUSCL approach [van Leer, 1979].

The so-called AUSMD [Wada and Liou, 1994] splitting is used, it reads

$$(\rho \bar{u}^\xi)_{1/2} = \bar{u}_L^{\xi+} \rho_L + \bar{u}_R^{\xi-} \rho_R \tag{4}$$

for the mass flux. The splittings for  $\bar{u}_L^{\xi+}$ ,  $\bar{u}_R^{\xi-}$  are given as

$$\bar{u}_L^{\xi+} := \begin{cases} \alpha_L \left( \frac{(\bar{u}_L^{\xi+} + c_m)^2}{4c_m} - \frac{\bar{u}_L^{\xi+} + |\bar{u}_L^{\xi+}|}{2} \right) + \\ \frac{\bar{u}_L^{\xi+} + |\bar{u}_L^{\xi+}|}{2}, \text{ if } \frac{\bar{u}_L^{\xi+}}{c_m} \leq 1 \\ \frac{\bar{u}_L^{\xi+} + |\bar{u}_L^{\xi+}|}{2}, \text{ otherwise} \end{cases} \tag{5}$$

$$\bar{u}_R^{\xi-} := \begin{cases} \alpha_R \left( -\frac{(\bar{u}_R^{\xi-} - c_m)^2}{4c_m} - \frac{\bar{u}_R^{\xi-} - |\bar{u}_R^{\xi-}|}{2} \right) + \\ \frac{\bar{u}_R^{\xi-} - |\bar{u}_R^{\xi-}|}{2}, \text{ if } \frac{\bar{u}_R^{\xi-}}{c_m} \leq 1 \\ \frac{\bar{u}_R^{\xi-} + |\bar{u}_R^{\xi-}|}{2}, \text{ otherwise} \end{cases} \tag{6}$$

with

$$\alpha_L = \frac{2(p/\rho)_L}{(p/\rho)_L + (p/\rho)_R} \tag{7}$$

$$\alpha_R = \frac{2(p/\rho)_R}{(p/\rho)_R + (p/\rho)_L} \tag{8}$$

and  $c_m = \max(a_L, a_R)$ . Note that  $\bar{u}^\xi$  on the right hand side of the equations (5) and (6) denote the contravariant velocity [Höhn,

2000].

Secondly, the pressure flux is

$$p_{1/2} = p_L^+ + p_R^-, \quad (9)$$

where

$$p^{+/-} = \begin{cases} \frac{1}{4} p_{L/R} \left( \frac{u_{L/R}^{\xi+/-}}{c_m} \pm 1 \right)^2 \left( 2 \mp \frac{u_{L/R}^{\xi+/-}}{c_m} \right) \\ \quad \text{if } \frac{u_{L/R}^{\xi+/-}}{c_m} \leq 1 \\ p_{L/R} \frac{u_{L/R}^{\xi+/-} \pm |u_{L/R}^{\xi+/-}|}{2u_{L/R}^{\xi+/-}}, \text{ otherwise} \end{cases} \quad (10)$$

The present method is easier to implement, computationally less expensive than the flux difference splitting methods, but has in the boundary layer still the same accuracy [Bergamini and Cinella, 1994]. Moreover, there is no need to specify a numerical dissipation in the code due to the upwind formulation.

### Discretization of the Viscous Terms

The second order partial derivatives appearing in the stress tensor components and the heat transfer terms of equation (2) correspond to a second order accurate central difference in which second derivatives are treated as differences across cell interfaces of first order derivative terms, as

$$\partial_\eta S \approx \delta_\eta S_{i,j} = (S_{i,j+1/2} - S_{i,j-1/2}). \quad (11)$$

The term

$$\tau_{xx} = \frac{2}{3} \mu \left( 2 \frac{\partial u}{\partial x} - \frac{\partial v}{\partial y} \right) \quad (12)$$

applying the chain rule becomes

$$\tau_{xx} = \frac{2}{3} \mu J \left( 2 \left( \frac{\partial u}{\partial \xi} y_\eta - \frac{\partial u}{\partial \eta} y_\xi \right) - \left( -\frac{\partial v}{\partial \xi} x_\eta + \frac{\partial v}{\partial \eta} x_\xi \right) \right) \quad (13)$$

and is differenced in  $S_{i,j+1/2}$  as

$$\tau_{xx} = \frac{2}{3} \mu_{i+1/2,j} J_{i+1/2,j} \left[ 2 \left( \delta_\xi u_{i+1/2,j} y_{\eta_{i+1/2,j}} - \delta_\eta u_{i+1/2,j} y_{\xi_{i+1/2,j}} \right) - \left( -\delta_\xi v_{i+1/2,j} x_{\eta_{i+1/2,j}} + \delta_\eta v_{i+1/2,j} x_{\xi_{i+1/2,j}} \right) \right] \quad (14)$$

with  $\delta_\eta u_{i,j+1/2} = u_{i,j+1} - u_{i,j}$ .

### Time Discretization

The Runge-Kutta four-step integration scheme which is used for the steady state and the unsteady equations, is second order accurate in time [Höhn, 2000]. The steady computations as well as the unsteady computations using reflecting boundary conditions are performed on a parallel computer (IBM-SP2) with a parallel version of the code using MPI. For the steady computations local time stepping is applied.

For the unsteady computations using non-reflecting boundary conditions an implicit factorized scheme [Beam and Warming, 1978] is applied on a single processor computer.

The implicit scheme, which has first order accuracy in time, follows to:

$$\begin{aligned} & \left( I + \Delta\tau \frac{\partial}{\partial \xi} \left( \frac{\partial \bar{F}}{\partial \bar{U}} \right)^n \right. \\ & \left. - \Delta\tau \frac{\rho_{-\infty}^* q_{-\infty}^*}{Re_{-\infty}} \frac{\partial}{\partial \xi} \left( \frac{\partial \bar{R}_1}{\partial \bar{U}} \right)^n \right) \\ & \left( I + \Delta\tau \frac{\partial}{\partial \eta} \left( \frac{\partial \bar{G}}{\partial \bar{U}} \right)^n \right. \\ & \left. - \Delta\tau \frac{\rho_{-\infty}^* q_{-\infty}^*}{Re_{-\infty}} \frac{\partial}{\partial \eta} \left( \frac{\partial \bar{S}_2}{\partial \bar{U}} \right)^n \right) \\ & (\bar{U}^{n+1} - \bar{U}^n) \\ & = -\Delta\tau \left( \frac{\partial}{\partial \xi} (\bar{F})^n + \frac{\partial}{\partial \eta} (\bar{G})^n \right. \\ & \left. - \frac{\rho_{-\infty}^* q_{-\infty}^*}{Re_{-\infty}} \left( \frac{\partial}{\partial \xi} (\bar{R})^n + \frac{\partial}{\partial \eta} (\bar{S})^n \right) \right. \\ & \left. + \frac{\partial}{\partial \xi} (\Delta \bar{R}_2)^n + \frac{\partial}{\partial \eta} (\Delta \bar{S}_1)^n \right) \end{aligned} \quad (15)$$

The Jacobian matrix  $\left( \frac{\partial \bar{F}}{\partial \bar{U}} \right)^n$  is developed with respect to the extrapolated variables  $U_L^+$  and  $U_R^-$  as

$$\begin{aligned} & \left( \frac{\partial \bar{F}}{\partial \bar{U}} \right)^n (\bar{U}^{n+1} - \bar{U}^n) \\ & = \left( \frac{\partial \bar{F}}{\partial \bar{U}_R} \right)^n (\bar{U}_R^{n+1} - \bar{U}_R^n) \\ & + \left( \frac{\partial \bar{F}}{\partial \bar{U}_L} \right)^n (\bar{U}_L^{n+1} - \bar{U}_L^n) \end{aligned} \quad (16)$$

The same treatment is applied to the other Jacobian matrices. The fluxes used on the left hand side of the implicit scheme are extrapolated with first order following the MUSCL approach which leads to a tridiagonal system. On the right hand side the

inviscid fluxes are extrapolated with second order accuracy to the cell face.

The terms  $\bar{R}_2$  and  $\bar{S}_1$  representing the viscous terms including cross derivatives with respect to  $\xi$  and  $\eta$  are lagged in time.

The present method can be easily extended to 3D. All details of the present method can be found in Höhn [2000].

## RESULTS

First the results for steady state flow are presented. After that unsteady results are presented for a compressor cascade case. The results obtained by the present method are always denoted with INSTHPT<sup>1</sup>.

### Steady State Results

**Viscous laminar calculations on a flat plate** The figure 1 shows the velocity distribution in comparison with the Blasius solution for a Reynolds number of 1 000 000 at a certain position on the plate. This flow case is characterized by sharp gradients perpendicular to the streamwise velocity direction near the wall. Nevertheless, the AUSM-scheme is able to resolve these gradients with a reasonable accuracy in contrast to the results which can be obtained with the classical van Leer flux splitting scheme [Höhn, 2000], where the high production of artificial viscosity in the viscous boundary layer leads to fuller velocity profiles.

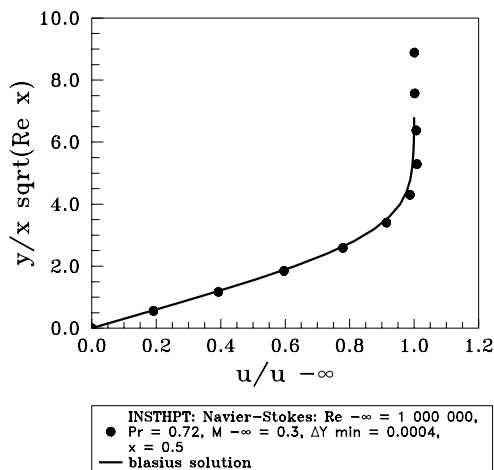


Figure 1. Velocity distribution on a flat plate  $Re = 1000000$ ,  $100 \times 100$  meshpoints

**Viscous turbulent calculations on a flat plate** Figure 2 shows the velocity profile for the turbulent boundary layer

close to the wall, at two positions on the plate, against the 'laminar' sublayer and the law of the wall. Again, the agreement is reasonably good.

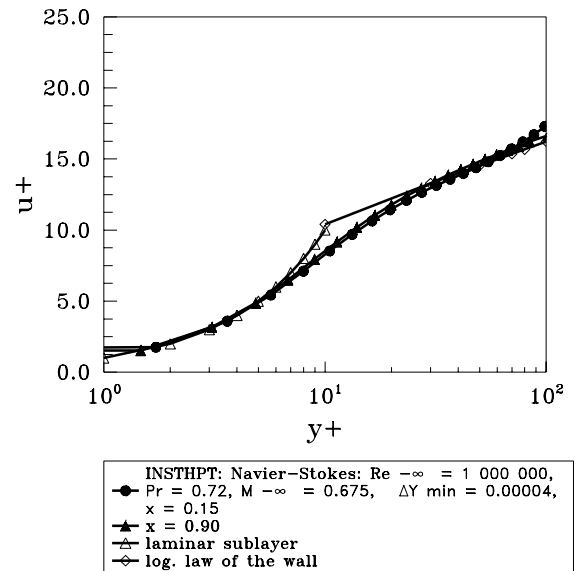


Figure 2.  $u^+ = f(y^+)$  on a flat plate  $Re = 1000000$  in comparison with the "log law" of the wall and the law for the "laminar" sublayer,  $100 \times 100$  meshpoints

**Steady state viscous, laminar flow around a 2D-cylinder** In order to study the separational behavior of the laminar code, this test case was chosen. Diagram 3 shows the separation angle  $\theta$  and the length of the separation bubble  $L/D$  for different Reynolds numbers  $Re_D$  against results obtained by other authors, here Dennis and Chang [1970] and Bouard and Coutanceau [1980]. Both, the separation point and the length of the separation bubble are reasonably predicted.

**Stcf 5 (Standard Configuration 5)** This two-dimensional cascade was investigated at the Office National d'Etudes et de Recherche Aéronautiques (ONERA). The configuration consists of six fan stage tip sections [Soize, 1992].

**4 degrees incidence** Figure 4 shows the cascade geometry and the mesh used for the calculations of the program INSTHPT with 80 points on the blade on the upper and the lower side, respectively and  $120 \times 100$  meshpoints in total. The Reynolds number based on the inlet velocity and the chord length is 1400000 for this flow case [Fransson and Verdon, 1993].  $Y^+$  is about 1.5 close to the leading edge for the calculations conducted with INSTHPT.

The results for steady state viscous flow shown in figure 5, the steady state pressure distribution, agree with VOLFAP<sup>2</sup>

<sup>1</sup>The blade flutter code INST-HPT is developed at the Chair of Heat and Power Technology, Royal Institute of Technology in Stockholm, Sweden.

<sup>2</sup>The viscous blade flutter code VOLFAP was developed at VOLVO Aero Copyright © 2001 by ASME

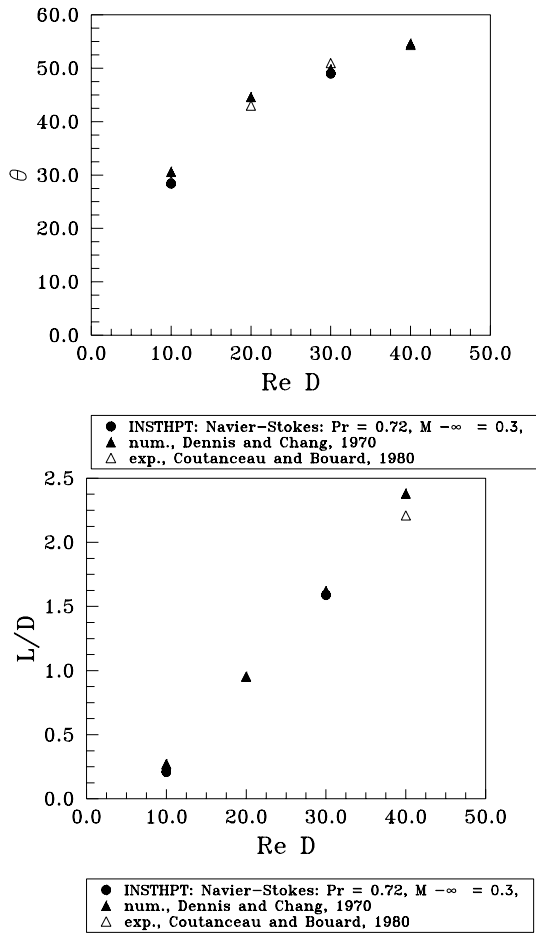


Figure 3. Separation angle and length of the separation bubble in comparison with other authors, 106 x 100 meshpoints

[Sidén, 1991]. Both calculations are conducted with an incidence angle of 4 degrees, i.e. the value measured in the experiments. However, a difference to the experimental data (see Bölcs and Fransson [1986]) is found. Predictions of another viscous flow solver VOLSOL<sup>3</sup> (see Groth et al. [1996]) conducted with an angle of incidence of 3.1 degrees show a better agreement with the experimental data. This is confirmed by other researchers as well. Hedberg [1994] performed calculations with the Q3D code VOLFAP varying the streamtube thickness. The numerical results could not match the experiments. However, by decreasing the angle of incidence to 2.5 degrees using the potential method FINSUP [Bölcs and Fransson, 1986] and 3.1 degrees with the present viscous method [Höhn, 2000] good agreement with the experiments can be achieved.

Figure 6 shows the length of the separation bubble against

Corporation. The used scheme applies central differences incl. artificial viscosity for the discretization of the governing equations.

<sup>3</sup>VOLSOL is a multipurpose code for inviscid and viscous flow and presently developed at VOLVO Aero Corporation. An upwind scheme is used for the discretization of the governing equations.

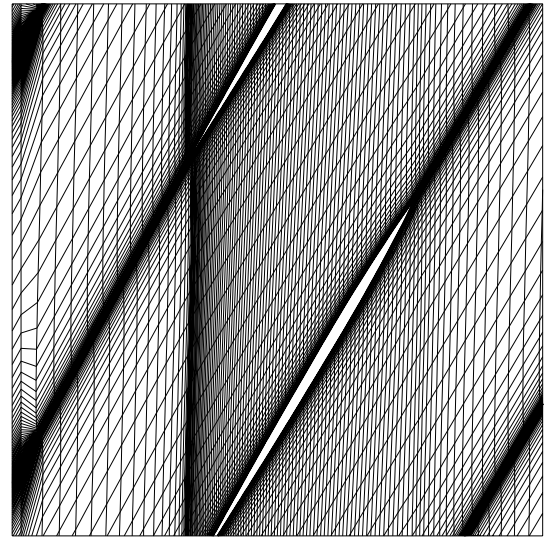


Figure 4. Mesh used for standard configuration 5, 120 x 100 meshpoints

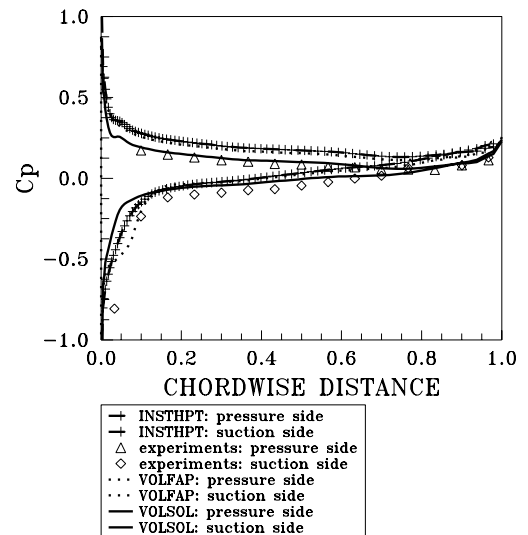


Figure 5. Steady state surface pressure distribution of standard configuration 5, case 2

the angle of incidence. Comparison is made again with VOLSOL [Groth et al., 1996] and VOLFAP [Sidén, 1991] and good agreement is found. VOLSOL seems to predict smaller separation bubbles than the other two codes especially for small angles of incidence. The computations for all three codes are performed with the turbulence model of Baldwin and Lomax [1978]. Values for higher angles of attack than six degrees are not shown in the diagram because for eight degrees incidence angle the flow is completely separated in the predictions of INSTHPT and more or less fully separated in the results obtained with VOLSOL.

**10 degrees incidence** This case is characterized by a complete separation of the flow on the suction side of the blade in the com-

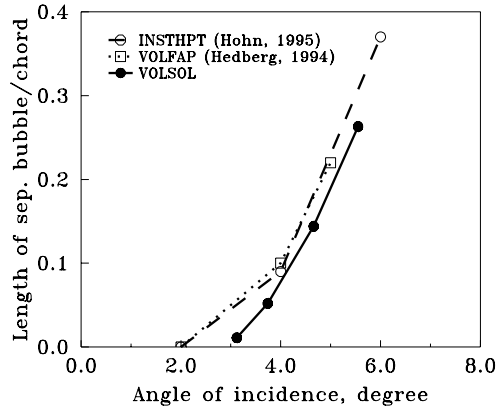


Figure 6. Length of the separation bubble against the angle of incidence, standard configuration 5

putations as well as in the experiments. The numerical results for steady state viscous flow presented in figure 7 show higher pressure values than measured in the experiments, though the back pressure from the experiments is taken for the numerical calculations. Lower values could be achieved by decreasing the angle of incidence as in the previous case. So far no other numerical data

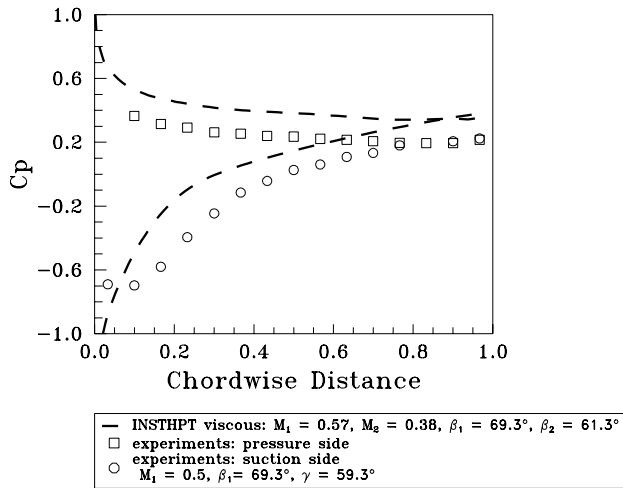


Figure 7. Steady state surface pressure distribution of standard configuration 5, case 18,  $i = 10^\circ$

is published on this case. Further investigations should show if a better agreement with the experiments can be achieved when the calculations are performed with a lower inlet Mach number (according to the experiments). However, the present study uses the values given by Fransson and Verdon [1993].

**Baldwin Lomax turbulence model for separated flow** Boussinesq [1877] introduced an analogy for the turbulent stresses similar to the viscous, laminar stresses. He described the turbulent shear stress  $\bar{u}v$  as a product of the turbulent viscosity  $\nu_t$

and the velocity gradient perpendicular to the mean flow:

$$\bar{u}v = -\nu_t \frac{\partial U}{\partial y} \quad (17)$$

One can show that this assumption does not account for rotational effects. This is the major drawback of the models based on the Boussinesq assumption. The Baldwin Lomax turbulence model is based on this assumption and can therefore not really describe rotational turbulent flow, i.e. the turbulent viscosity  $\nu_t$  in turbulent separated flow.

The Baldwin and Lomax turbulence model is a two-layer, zero equation (algebraic) model. It is patterned after the Cebeci-Smith model [Cebeci and Smith, 1974] and introduces a modification that eliminates the need to search for the edge of the boundary layer to determine the length scale. Its strength and weakness are well known in the CFD community; it predicts accurately the steady flows with little or no separation and performs poorly if there is large separation, either shock-induced or otherwise.

Despite its disadvantages the model is used as a first step, because of its simple implementation and the fact that it is computationally less expensive than one equation or two equation models, like the k- $\epsilon$  turbulence model [Höhn, 2000].

**Convergence** Convergence for the steady state computations is achieved when the maximum value for the change of density during one time step has a drop of about  $10^5$  to  $10^7$  depending on the flow case.

For the steady state viscous computations mesh sensitivity studies have been performed to ensure that the solution is independent of the mesh resolution.

## Unsteady Results

**4 degrees incidence** The shown unsteady viscous flow situation is case 7 of standard configuration 5 according to Fransson and Verdon [1993]. The cascade is forced into a pure torsional vibration mode of a frequency of 550 Hz and an amplitude of  $0.1^\circ$  with an interblade phase angle of  $180^\circ$  and a reduced frequency of 2.04 based on full chord. The steady state initial solution used is characterized by an incidence angle of  $4^\circ$  and an inlet Mach number of 0.5, see above. As the figures 8 and 9 show, the results for the unsteady amplitude and phase of the surface pressure distribution are in reasonable agreement with experiments presented by Fransson and Verdon [1993]. The results are based on the fundamental Fourier coefficient of the unsteady pressure obtained by a Fourier analysis in time. The viscous computation is performed with the explicit parallelized unsteady version of the code on an IBM SP2 [Höhn, 1996]. The inviscid code, using the

same capacitive boundary conditions and running for 12 cycles as well (which is found to be sufficient for an unsteady periodic solution), shows on the pressure side (LS) as expected no big difference to the viscous code for the unsteady amplitude. The difference in the leading edge region is due to a coarser mesh for the inviscid solution. The used mesh had  $80 \times 40$  mesh points for the inviscid computations. On the other hand, the suction side shows a big difference, which is expected due to the fact that separation occurs in the viscous solution. Since the results are compared with the experiments where only one blade is excited<sup>4</sup>, a comparison with the Navier-Stokes code VOLFAP [Sidén, 1991] is made under the same conditions as for the results obtained with the present method. The results obtained with VOLFAP [Sidén, 1991] by Hedberg [1994], see figure 8, agree well with the present viscous method on the pressure side but generally have higher amplitudes for the unsteady pressure amplitude on the suction side, especially close to the leading edge where separation occurs. The results agree fairly well in phase with the present method for the suction side as well as for the pressure side, as it can be seen in figure 9.

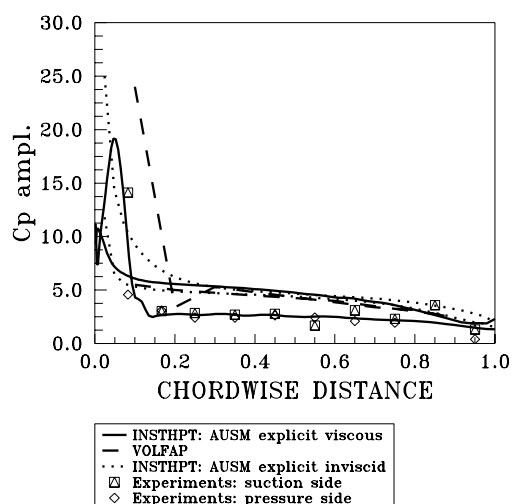


Figure 8. Amplitude of the unsteady pressure over chord for standard configuration 5 case 7,  $i = 4^\circ$ , reflecting boundary conditions applied in INSTHPT

Figure 10 and figure 11 show the unsteady pressure with respect to amplitude and phase for case 7 for INSTHPT and VOLFAP. The viscous and inviscid results for INSTHPT are obtained using the implicit time marching method with non-reflecting

<sup>4</sup>Consequently, the experiments show only the eigeninfluence of the blade on itself, which is shown to be the biggest contribution [Bölcs and Fransson, 1986]. The movement of the neighboring blades in the numerical predictions give only a minor contribution on the amplitude of the unsteady pressure distribution and almost no influence on the unsteady phase [Bölcs and Fransson 1986]. Therefore, the computation with two passages and an interblade phase angle of 180 degrees is a good approximation.

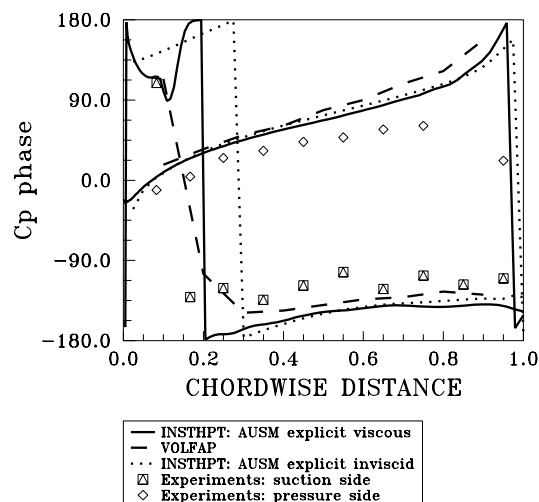


Figure 9. Phase of the unsteady pressure over chord for standard configuration 5 case 7,  $i = 4^\circ$ , reflecting boundary conditions applied in INSTHPT

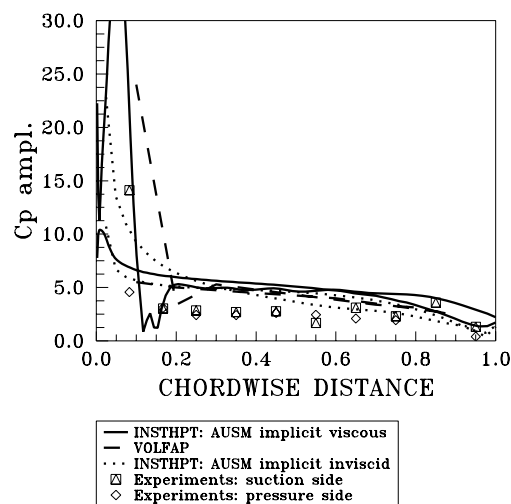


Figure 10. Amplitude of the unsteady pressure over chord for standard configuration 5 case 7,  $i = 4^\circ$ , nonreflecting boundary conditions applied in INSTHPT

boundary conditions. In general, good agreement with VOLFAP is found with respect to the prediction of the unsteady amplitude and phase.

Comparing these results with the results obtained by the parallel, viscous, explicit version of the code using capacitive (non-reflecting) boundary conditions, see figures 8 and 9, one can see that the unsteady pressure amplitude is higher for the calculations using non-reflecting boundary conditions, especially on the suction side of the blade. The predicted phase is almost the same for the computations performed with the explicit viscous unsteady version of INSTHPT and the implicit viscous unsteady version of INSTHPT, which leads to the conclusion that the influence of the boundary conditions, i.e. the use of reflecting or non-

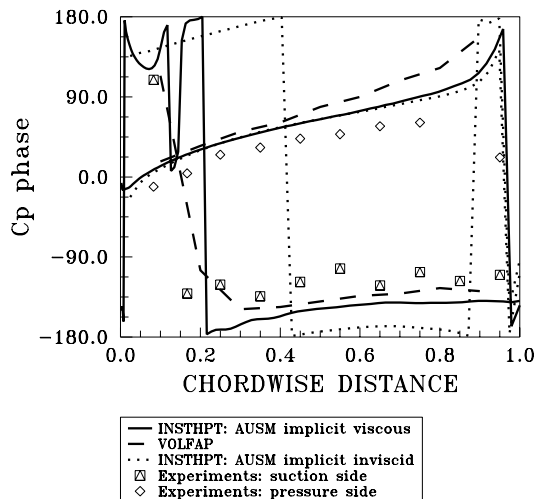


Figure 11. Phase of the unsteady pressure over chord for standard configuration 5 case 7,  $i = 4^\circ$ , nonreflecting boundary conditions applied in INSTHPT

reflecting boundary conditions, is significant on the suction side of the blade for this particular test case.

**10 degrees incidence** This present unsteady viscous flow situation is case 18 of standard configuration 5 according to Fransson and Verdon [1993]. Based on the steady state initial solution which is characterized by an incidence angle of  $10^\circ$  and an inlet Mach number of 0.5 and given in the previous steady state section, the cascade is forced into a pure torsional vibration mode of a frequency of 550 Hz and an amplitude of  $0.1^\circ$  with an interblade phase angle of  $180^\circ$  and a reduced frequency of 2.04 based on full chord.

Figure 12 shows the amplitude of the unsteady surface pressure obtained on the suction and the pressure side of the blade in comparison with experiments [Fransson and Verdon, 1993] based on a Fourier decomposition in time for the first harmonic. On the suction side the separated flow causes a peak in the unsteady pressure amplitude which is shown in the experiments and weakly shown in the numerical predictions. In general the amplitudes are higher than for the experiments, which is probably due to the fact that only one blade is oscillating in the experiments [Bölcs and Fransson, 1986].

Figure 13 shows the phase of the unsteady surface pressure. The experimental results are considerably off on the suction side of the blade, whereas the pressure side is in good agreement with the experiments. Unfortunately, no published numerical data at all is available for this case.

**Damping** Figure 14 shows the computed aerodynamic damping as a function of the incidence angle for standard configuration 5 for the implicit inviscid and viscous codes of INSTHPT compared with the experimental data [Fransson and Verdon, 1993]

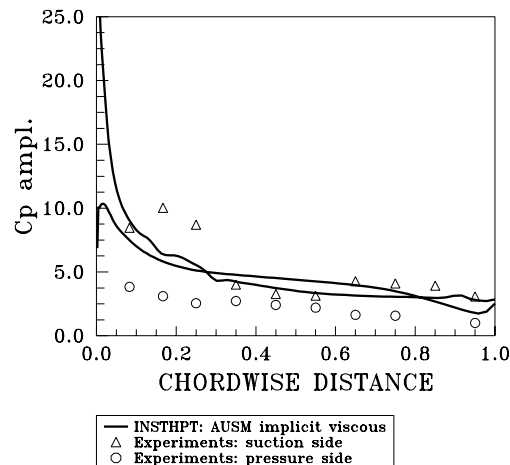


Figure 12. Amplitude of unsteady surface pressure distribution of standard configuration 5, case 18,  $i = 10^\circ$

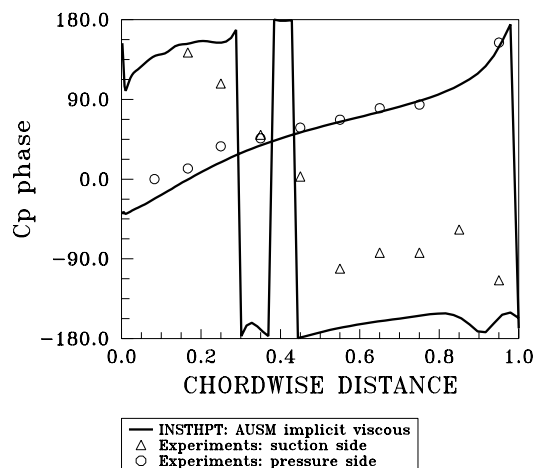


Figure 13. Phase of unsteady surface pressure distribution of standard configuration 5, case 18,  $i = 10^\circ$

and the inviscid code FINSUP [Hedberg, 1994] and the viscous code VOLFAP [Hedberg, 1994]. The tendency for the damping measured in the experiments is predicted by the viscous code INSTHPT. However, for small incidence angles (less than  $6^\circ$ ) lower damping values are predicted and for high angle of incidence higher positive damping rates are computed. The inviscid method of INSTHPT gives lower values for the damping than the viscous code of INSTHPT. The same tendency is shown by FINSUP and VOLFAP. No published numerical data is available for the angle of incidence of 7.5 and 10 degrees. In general the viscous predictions are more stable in an aeroelastic sense than the inviscid predictions for the present method. This is confirmed by the calculations performed by Hedberg [1994] with FINSUP and VOLFAP.

**Convergence and performance** Table 1 gives the most important convergence and performance data of the present numerical

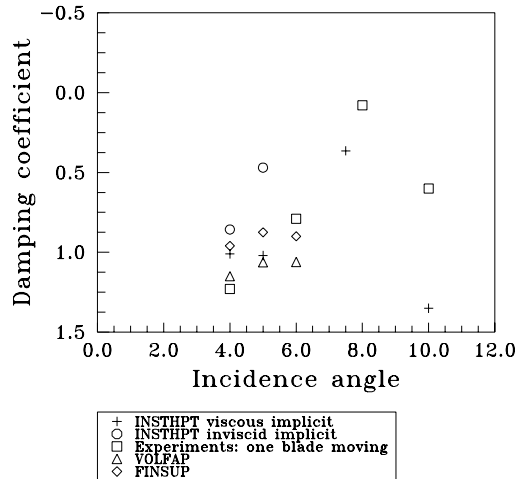


Figure 14. Damping as a function of incidence angle standard configuration 5

Case	CFL	iterat. / cycle	cycles * passages	CPU time * nodes [h]	expl. / impl.
7, invis.	0.2	5980	12	5	expl.
7, invis.	5.0	250	12	0.2	impl.
7, visc.	0.4	684710	12	1920	expl.
7, visc.	30	9120	12	25.6	impl.
18, visc.	20	13680	12	38.4	impl.

Table 1. International standard configuration 5

method for the unsteady computations. For STCF 5 case 7, for example, 25.6 h on a RS 6000 computer (160 MHz) were needed for the viscous, implicit computation on 2 blade passages. The change of the amplitude of the moment coefficient was less than 0.1 per cent after 6 cycles. This was assumed to be sufficient for an unsteady periodic flow.

High CFL numbers / less iterations for the implicit calculations led to an oscillation of the aeroelastic moment coefficient and had to be avoided.

## CONCLUSIONS

The present method shows generally good agreement for the investigated test cases in comparison with experiments and results obtained by other flow solvers for steady state flow conditions. This is shown for flat plate cases for laminar and turbulent flow and the laminar flow around a 2-D cylinder. Viscous steady state, fully turbulent, calculations for standard configuration 5 are shown. The predicted surface pressure coefficients and the

length of the separation bubble generally agree with the experiments and results obtained by other flow solvers.

Unsteady computations are performed on STCF 5 at the angles of incidences of  $4^\circ$ ,  $6^\circ$ ,  $8^\circ$  and  $10^\circ$ . In the separated regions the present method accounts for viscous effects, which is seen in the computed unsteady surface pressure distribution and the aeroelastic damping, and good agreement is found with other numerical methods [Siden, 1991; Whitehead, 1990]. The unsteady predictions for viscous flow show a higher damping coefficient than for the inviscid computations, which is in agreement with the results of other authors. The viscous predictions of the present method give a good agreement with the measured aeroelastic damping for STCF 5.

The unsteady results show that the present method can be used for massively separated stalled subsonic flow. However, the author is aware that the Baldwin-Lomax turbulence model is not the best choice for flow cases, where large separation occurs.

## ACKNOWLEDGMENT

I would like to express my gratitude to Professor Torsten H. Fransson at the Chair of Heat and Power Technology at the Royal Institute of Technology of Stockholm, who made this work possible.

The study was carried out in the beginning within the NUTEK project "Unsteady Flow Around Cascaded Blades at or Near Stall". Later the study was supported by the NFFP project "Aeromechanical Vibrations in Cascades". The financial support of ASEA Brown Boveri (CH), Volvo Aero Corporation AB (S), Rolls Royce plc. (UK) and NUTEK<sup>5</sup> (S) during the first project and FMV<sup>6</sup> (S) and VOLVO Aero Corporation (S) in the second project is gratefully acknowledged.

## REFERENCES

- Ayer, T. C. and Verdon, J. M.; 1996 "Validation of a Non-linear Unsteady Aerodynamic Simulator for Vibrating Blade Rows." ASME Paper 96-GT-340, 1996.
- Baldwin, B. and Lomax, H.; 1978 "Thin-Layer Approximation and Algebraic Model for Separated Turbulent Flow." AIAA Paper 78-257, 1978.
- Beam, R.M. and Warming, R.F.; 1978 "An Implicit Factored Scheme for the Compressible Navier-Stokes Equations.", AIAA Journal, Vol. 16, No. 4, April 1978.
- Bölcs, A.; Fransson, T. H.; 1986 "Aeroelasticity in Turbomachines, Comparison of Theoretical and Experimental Cascade Results.", Communication de Laboratoire de Thermique Appliquée et de Turbomachines, No. 1, Ecole Polytechnique Fédérale de Lausanne, Switzerland, 1986.

<sup>5</sup>Project manager: Dr. Wiktor Raldow, Project number: 91-00448P

<sup>6</sup>Project manager: Mr. Dag Brising, Project number NFFP-304

Bouard, R.; Coutanceau, M.; 1980 "The Early Stage of Development of the Wake Behind an Impulsively Started Cylinder for  $40 \leq Re \leq 10E4$ .", Journal of Fluid Mechanics, Vol. 101, pp. 583 - 607, 1980.

Boussinesq, T. V.; 1877 Mem. pres Acad. Sci., 3rd edn. Paris XXIII, p. 46, 1877.

Cebeci, T.; Smith, A. M. O.; 1974 "Analysis of Turbulent Boundary Layers.", Academic Press, New York, 1974.

Chakravarthy, S.R.; 1983 "Euler Equations - Implicit Schemes and Boundary Conditions.", AIAA Journal, Vol. 21, No. 5, April 1983.

Dennis, S.C.R.; Gau-Zu Chang; 1970 "Numerical Solution for Steady Flow Past a Circular Cylinder at Reynolds Numbers up to 100.", Journal of Fluid Mechanics, Vol. 42, pp. 471-489, 1970.

Fransson, T. H. and Pandolfi, M.; 1986 "Numerical Investigation of Unsteady Compressible Flow Through an Oscillating Cascade.", ASME Paper 86-GT-304, 1986.

Fransson, T. H. and Verdon, J.M.; 1993 "Standard Configurations for Unsteady Flow through Vibrating Axial-Flow Turbomachine Cascades.", in: Unsteady Aerodynamics, Aeroacoustics and Aeroelasticity of Turbomachines and Propellers, H.M. Atassi (ed.), Springer-Verlag, New York, pp. 859 - 889, 1993.

Groth, J. P., Martensson, H. and Eriksson, L.-E.; 1996 "Validation of a 4D Finite Volume Method for Blade Flutter.", ASME Paper 96-GT-429, ASME Turbo Expo, 1996.

Grüber, B.; Carstens, V.; 1996 "Computation of the Unsteady Transonic Flow in Harmonically Oscillating Turbine Cascades Taking Into Account Viscous Effects.", ASME-Paper 96-GT-338, 1996.

Hedberg, K.; 1994 "Validation of Flutter Prediction Models.", Master of Science Thesis, Royal Institute of Technology, Chair of Heat and Power Technology, Stockholm, 1994.

Höhn, W.; 1996 "Unsteady Viscous Flow Around Cascaded Vibrating Blades at or Near Stall.", "Teknologi-Licenciat"-Thesis, Royal Institute of Technology, Chair of Heat and Power Technology, Stockholm, 1996.

Höhn, W.; 2000 "Numerical Investigation of Blade Flutter at or Near Stall in Axial Turbomachines.", "PhD-Thesis, Royal Institute of Technology, Chair of Heat and Power Technology, ISBN 91-7170-516-3, Stockholm, 2000.

Huff, D.L., Swafford, T.W. and Reddy, T.S.R.; 1991 "Euler Flow Predictions for an Oscillating Cascade Using High Resolution Wave-Split Scheme.", ASME-Paper 91-GT-198, 1991.

Ott, P.; 1991 "Oszillierender senkrechter Verdichtungsstoss in einer ebenen Duese.", Thèse No. 985, Ecole Polytechnique Fédérale de Lausanne, 1991.

Sidén, L. D. G.; 1991 "Numerical Simulation of Viscous Compressible Flow Applied to Turbomachinery Blade Flutter.", Ph. D. Thesis, Chalmers University of Technology, Gothenburg, Sweden, 1991.

Soize, C.; 1992 "Strong Coupling between Inviscid Fluid

and Boundary Layer for Airfoils with a Sharp Edge.", Rech. Aérosp., No. 1992-3, France.

van Leer, B.; 1979 "Towards the Ultimate Conservative Difference Scheme, A Second Order Sequel to Godunov's Method.", Journal of Computational Physics, Vol. 32, pp. 101 - 136.

Wada, Y. and Liou, M. S.; 1994 "A Flux Splitting Scheme with High-Resolution and Robustness for Discontinuities.", AIAA Paper 94-0083, 1994.

Weber, S., Benetschik, H., Peitsch, D. and Gallus, H.E. ; 1997 "A Numerical Approach to Unstalled and Stalled Flutter Phenomena in Turbomachinery Cascades.", ASME Paper 97-GT-102.

Whitehead, D.S.; 1990 "A Finite Element Solution of Unsteady Two-Dimensional Flow in Cascades.", Int. Journal of Numerical Methods in Fluids, Vol. 10, 1990.

Wilcox, D. C.; 1993 "Turbulence Modeling for CFD.", 1st. edition, DCW Industries, La Canada, California, 1993.